Catalysis Science & Technology

ROYAL SOCIETY OF CHEMISTRY

PAPER

View Article Online
View Journal | View Issue

Cite this: *Catal. Sci. Technol.*, 2023, **13**, 2142

Consequence of products from oxidative coupling of methane in a non-oxidative high temperature environment†

Haruka Komada,[a] Keisuke Obata,[a] Duanxing Li,[a] S. Mani Sarathy[bc] and Kazuhiro Takanabe*[ad]

Received 21st December 2022,
Accepted 18th February 2023

DOI: 10.1039/d2cy02145e

rsc.li/catalysis

Oxidative coupling of methane (OCM) is a direct process that converts methane to higher hydrocarbons, such as ethylene. For several decades, various catalysts and their reaction mechanisms have been investigated to obtain high selectivity for the target products. However, the consequences of OCM products after O_2 depletion at high temperatures, which is generated by an exothermic reaction, have been often overlooked. In the present study, a two-stage reactor that mimics an industrial reactor was used to study the successive reactions of OCM products. Gas phase homogeneous and heterogeneous reactions on the surface of catalysts and supports have been systematically investigated. Dehydrogenation of OCM products to acetylene and the following condensation occurs in the gas phase. Meanwhile, steam reforming of OCM products concurrently followed by water gas shift reactions was observed on various catalysts and supports and led to the loss of C_2 yield. Based on the investigations, a design guideline for the OCM reactor is proposed.

Introduction

Olefins, such as ethylene, propylene, and butadiene, are important chemical feedstocks in the manufacturing process of various functional compounds, such as plastics and rubbers. Currently, olefins are obtained by refining crude oil followed by their cracking, and their demand is expected to increase continuously. Due to concerns about crude oil depletion, however, it is necessary to develop synthetic routes using other carbon sources. Methane is considered an alternative hydrocarbon source due to the recent shale gas revolution. The general synthetic route for obtaining olefins from methane involves at least three steps: (1) synthesis gas (syngas) generation through a methane reforming reaction, (2) methanol synthesis from syngas, and (3) methanol-to-olefin reaction.[1] Syngas is a mixture of H_2, CO, and some CO_2, which are the major intermediates in the industrial methane conversion process. The methods to obtain syngas include steam reforming, partial oxidation, and carbon dioxide reforming using H_2O, O_2, and CO_2 as reactants, respectively. The reaction equations for each reforming process are shown below.

$$CH_4 + H_2O \rightarrow CO + 3H_2 \quad \Delta H^0_{298K} = 206 \text{ kJ mol}^{-1} \quad (1)$$

$$CH_4 + 1/2O_2 \rightarrow CO + 2H_2 \quad \Delta H^0_{298K} = -36 \text{ kJ mol}^{-1} \quad (2)$$

$$CH_4 + CO_2 \rightarrow 2CO + 2H_2 \quad \Delta H^0_{298K} = 247 \text{ kJ mol}^{-1} \quad (3)$$

The indirect conversion process of CH_4 *via* syngas is an attractive process that is widely used at an industrial level. On the other hand, the syngas production process itself is costly and energy-intensive. In addition, the formation of hydrocarbons from synthesis gas requires either CO or H_2 to remove the oxygen from CO leading to a loss of carbon atom utilization efficiency or consumption of valuable H_2.[2] In short, the indirect route is a process involving oxygen addition to and removal from hydrocarbons. In contrast, oxidative coupling of methane (OCM), which can yield C_2 or higher olefins from methane in one step in the presence of oxygen,[2–4] has been attracting great attention for further improving the efficiency of the CH_4 conversion process. The

[a] *Department of Chemical System Engineering, School of Engineering, The University of Tokyo, 7-3-1 Hongo, Bunkyo-ku, Tokyo, 113-8656, Japan. E-mail: takanabe@chemsys.t.u-tokyo.ac.jp*
[b] *King Abdullah University of Science and Technology (KAUST), Clean Combustion Research Center (CCRC) and Physical Sciences and Engineering Division (PSE), 4700 KAUST, Thuwal 23955-6900, Saudi Arabia*
[c] *King Abdullah University of Science and Technology (KAUST), KAUST Catalysis Center (KCC), 4700 KAUST, Thuwal23955-6900, Saudi Arabia*
[d] *PRESTO, Japan Science and Technology Agency (JST), Kawaguchi, Saitama 332-0012, Japan*

† Electronic supplementary information (ESI) available. See DOI: https://doi.org/10.1039/d2cy02145e

advantage of the OCM reaction over conventional industrialized reactions is that OCM is an exothermic reaction (eqn (4)) and has no thermodynamic barriers due to negative changes in both enthalpy and Gibbs energy.

$$2CH_4 + 1/2O_2 \rightarrow C_2H_6 + H_2O \quad \Delta H^0_{298K} = -177 \text{ kJ mol}^{-1} \quad (4)$$

Unlike indirect conversion *via* synthesis gas, OCM has the potential to reduce conversion costs because of a reduction in the number of steps in the conversion process and the energy input.

Research concerning the OCM reaction started as early as the 1980s by Keller and Bhasin,[5] and the reaction is known to go through a complex homogeneous–heterogeneous reaction network between the intermediates on the surface of catalysts and gas phase radicals.[6,7] The widely accepted reaction mechanism of the OCM reaction is initiated by the dissociative adsorption of O_2 on the catalyst surface to form surface oxygen species O*. The surface oxygen species abstract hydrogen atom from CH_4 to form CH_3 radicals, which dimerize in the gas phase to produce C_2H_6 as the primary product. However, because the resulting hydrocarbons can be easily activated compared to CH_4 due to their weaker C–H bond strength, their overoxidation to CO_x is a challenge, which results in a loss of selectivity and the resulting yield at high CH_4 conversion.[8–10] Various catalysts, such as Li/MgO-, La_2O_3-, and Sm_2O_3-based catalysts, were investigated to improve the process's selectivity and reaction rate,[11–15] One of the most studied catalysts is alkali metal-based tungstate, such as Na_2WO_4, due to its high C_2 selectivity. The unique feature of the tungstate catalysts is that the addition of H_2O in the reactant stream improves the CH_4 conversion rate and the selectivity to C_2 products.[16,17] We have proposed that the OH radical is generated from H_2O and O_2 on the catalyst surface and that the resulting highly reactive OH radical readily abstracts the hydrogen atom from stable CH_4.[16–20] On the surface of the catalyst, alkali metal peroxides/superoxides were observed,[18] and these species are suggested to be involved in catalyzing the OH radical formation. The reported single-pass C_2 yield reached 25% using $Mn/Na_2WO_4/SiO_2$ catalysts at 850 °C,[21] which is close to the industrial target of ~30%. The C_{2+} yield in a sequential dual reactor with Na_2WO_4/SiO_2 reached 27.6% at 850–880 °C.[22]

Since OCM is an exothermic reaction as shown in eqn (4), the use of an adiabatic reactor is considered necessary to make the process more efficient *via* utilization of the reaction heat as thermal energy. However, the resulting gas mixture is predicted to reach a high temperature even above 1000 °C after complete depletion of O_2.[23] Although various studies have been devoted to developing selective catalysts and revealing their reaction mechanisms,[24–30] the consequences of OCM products exposed under non-oxidative high temperature conditions have often been overlooked. For example, ethane generated from the OCM reaction is reported to undergo dehydrogenation to ethylene in the later stages at high temperatures after O_2 depletion.[31,32]

$$C_2H_6 \rightarrow C_2H_4 + H_2 \quad \Delta H^0_{298K} = 136 \text{ kJ mol}^{-1} \quad (5)$$

Nevertheless, undesired reactions involving OCM products have not been previously discussed. In an industrial reactor, excess amounts of catalysts need to be introduced to compensate for the potential loss of activity, a process that would result in the exposure of the OCM products to the extra catalysts and supports at high temperatures due to their exothermicity. In this study, we systematically investigated successive reactions of OCM products under high temperature non-oxidative conditions using a two-stage reactor that mimics an industrial reactor (Fig. 1). The OCM reaction is completed in the first stage reactor, while the OCM product mixture is exposed to the high temperature non-oxidative conditions in the second stage so that the successive reactions can be investigated. Both the homogeneous gas phase and heterogeneous reactions on various supports and catalysts after O_2 depletion have been studied independently. Based on the present investigation, a design guideline for an OCM reactor that can achieve a high C_2 yield is proposed.

Experimental

Catalyst preparation

A wet impregnation method was used to prepare 5 wt% Na_2WO_4/SiO_2 using $Na_2WO_4{\cdot}2H_2O$ (≥99%, Sigma-Aldrich) as a

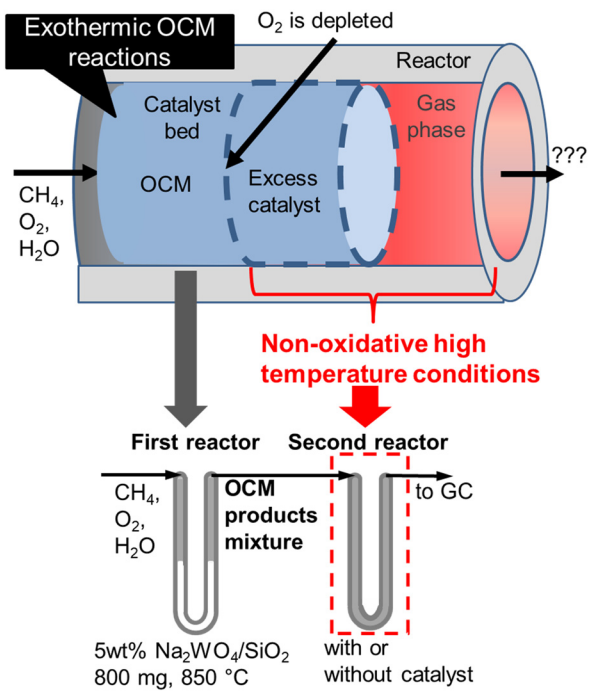

Fig. 1 Schematic representation of the two-stage reactor that mimics industrial reactors.

precursor on a SiO_2 support (Sigma-Aldrich, Silica gel, Davisil Grade 643, pore size 150 Å, 200–425 mesh), followed by calcination in air at 900 °C for 8 h. Al_2O_3 (Sigma-Aldrich, α-phase, −100 mesh) and ZrO_2 (RC-100, 99.5%, Daiichi Kigenso Kagaku Kogyo) supports were used as received. Cristobalite-phase SiO_2 was obtained by heating the above-mentioned SiO_2 at 900 °C in air for 8 h. All samples were sieved after pelletization to obtain aggregates in a size range of 0.25 to 0.5 mm.

Catalytic performance evaluation

All activity tests were performed using a U-shaped quartz flow reactor (6 mm O.D., 4 mm I.D.) heated using an electric furnace (temperature distribution is shown in Fig. S1†). The catalyst bed was held between two plugs of quartz wool, and the thermocouple was located outside the quartz tube close to the catalyst bed to control the furnace temperature. CH_4 (>99.999%) and O_2 (20.0% diluted by Ar) were used as reactants, and Ar (>99.9999%) was used as a diluent. Mass flow controllers (Brooks) were used to obtain the desired gas composition and flow rate. A saturator with a temperature-controlled water jacket (15 °C) was used to introduce 1.7 kPa H_2O in the reactant stream. The concentrations of the reactants and products were measured using an online gas chromatograph (Shimadzu GC-2014) equipped with a flame ionization detector ([FID] for hydrocarbon products) and a thermal conductivity detector ([TCD] for H_2, O_2, CO, and CO_2), which are connected to GS-Gaspro and Shincarbon columns, respectively. All reactants and products passed through a water vapor trap that was located before the GC. The schematic image of the two-stage reactor is shown in Fig. 1, in which the OCM gas products from the first reactor were directly introduced into the second reactor. The reactor's furnace temperatures were controlled independently.

The conversion of methane and the selectivity to each carbon product and H_2 were calculated as shown below.

$$\mathrm{CH_4\ conversion\,(\%)} = \frac{\text{Total moles of carbon in all products}}{\text{Total moles of carbon in all products} + \text{outlet } \mathrm{CH_4}} \times 100 \quad (6)$$

$$\mathrm{C_{2-7}\ selectivity\,(\%)} = \frac{\text{Total moles of carbon in } \mathrm{C_{2-7}} \text{ products}}{\text{Total moles of carbon in all products}} \times 100 \quad (7)$$

$$\mathrm{H_2\ selectivity\,(\%)} = \frac{\text{Moles of } \mathrm{H_2}}{2 \times (\text{Total moles of carbon in all products})} \times 100 = \frac{\text{Total moles of hydrogen in } \mathrm{H_2}}{\text{Total moles of hydrogen in } \mathrm{H_2}, \mathrm{C_{2+}} \text{ products, and } \mathrm{H_2O}} \times 100 \quad (8)$$

The H_2 selectivity in this study defines the percentage of the measured H_2 relative to the hydrogen in the converted CH_4 or relative to all the hydrogen in the products containing hydrogen.

Simulation of homogeneous gas phase reactions

Only the gas phase reactions of the OCM products are simulated without surface reactions. Simulations were performed using a plug-flow reactor model with the CHEMKIN software [ANSYS CHEMKIN-PRO v. 17.2, 2018] by varying the residence times and isothermal temperatures. The gas-phase chemical kinetic model is KAUST-Aramco PAH Mech 1-GS (KAM1-GS), which contains 574 species and 3379 reactions.[33–35] OCM product mixtures, with experimentally obtained gas composition from the outlet of the first reactor, were fed to the inlet in the simulation.

Results and discussion

Selectivity under various O_2 depletion conditions

In the present study, 5 wt% Na_2WO_4/SiO_2 is used as a model OCM catalyst due to its high C_2 selectivity. C_2 selectivity in a single reactor after O_2 depletion was firstly investigated at various temperatures and residence times under dilute conditions (P_{CH_4} = 10 kPa, P_{O_2} = 1.7 kPa, and P_{H_2O} = 1.7 kPa), as shown in Fig. 2.

CH_4 conversion remained constant at approximately 22% under the studied conditions. C_{2+} selectivity was 80% at a furnace temperature of 850 °C and a residence time of 0.3 s, which is comparable to the results from a previous report.[19] However, the H_2, C_2H_2, C_2H_4, and CO_x selectivities increased

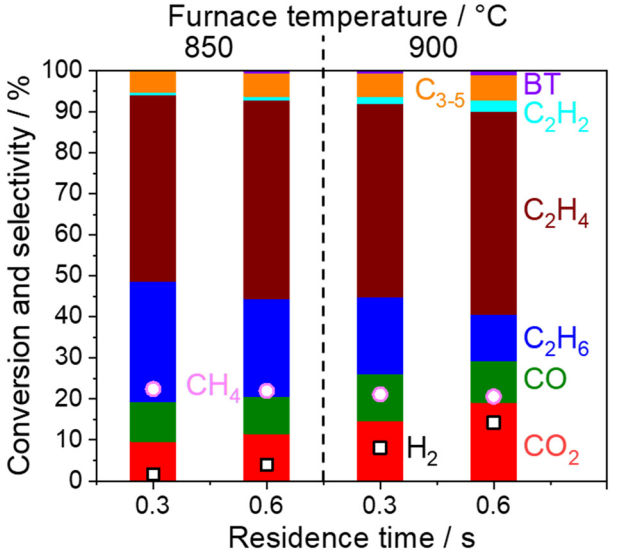

Fig. 2 Product distribution and CH_4 conversion measured with a single quartz tube reactor using 800 mg of 5 wt% Na_2WO_4/SiO_2 under O_2 depletion conditions (850 or 900 °C, CH_4 10 kPa, O_2 1.7 kPa, H_2O 1.7 kPa, total pressure 101 kPa, Ar balance, 40 or 80 mL min^{-1}). The residence time was calculated by using the volume occupied by the catalysts in the quartz tube. BT denotes benzene and toluene.

while the C_2H_6 selectivity decreased at higher furnace temperatures and residence times, which indicates the presence of successive reactions of OCM products. Homogeneous gas phase reactions and heterogeneous surface reactions may occur at high temperatures. To clarify their contributions in the successive reactions of OCM products, a two-stage reactor, which mimics an industrial reactor, was used as shown in Fig. 1. The OCM reaction was first completed, which means that O_2 was depleted in the first reactor using 800 mg of the model catalyst, 5 wt% Na_2WO_4/SiO_2. The product gas mixture was further introduced to the second reactor in which the temperature could be controlled independently from that in the first reactor. The difference in gas compositions between the outlets from the first and second reactors allowed us to investigate the successive reactions of OCM products in non-oxidative environments. The homogeneous gas phase reactions were investigated without loading catalysts in the second quartz tube reactor, while the heterogeneous surface reactions were studied by loading various catalysts and supports into the reactor.

Contributions from homogenous gas phase reactions

Homogeneous reactions of the product gas mixture from the first stage OCM reactor were investigated using an empty quartz tube in the second reactor at high temperatures as shown in Fig. 3.

First, the result on the left side in Fig. 3 is the selectivity and conversion at the outlet from the first reactor. Full conversion of O_2 was confirmed under the reaction at 850 °C, where the first reactor is shown in Fig. S2.† When the outlet gas from the first-stage reactor was introduced into the second reactor, the C_2H_6 and C_2H_4 selectivities decreased, while the C_2H_2 selectivity increased while increasing the furnace temperature. Considering that H_2 selectivity also increased after O_2 was already depleted, the dehydrogenation of C_2 products seemed to have occurred in the gas phase as shown in eqn (5) and (9).

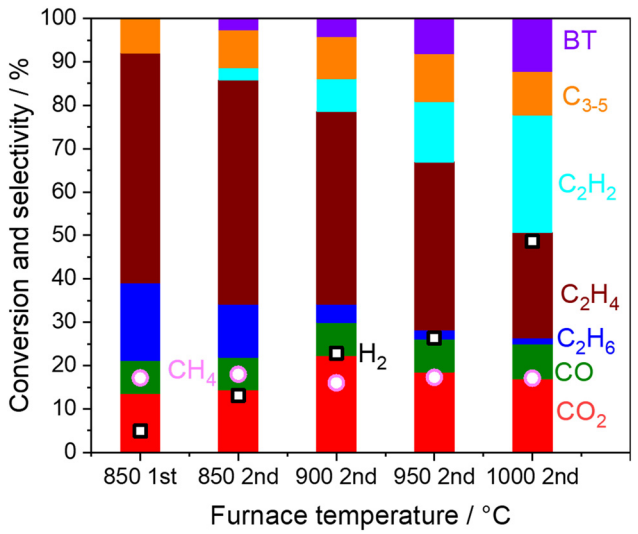

Fig. 3 Product distribution and CH_4 conversion from the outlets of the first and the second reactor. Inlet gas; CH_4 10 kPa, O_2 1.4 kPa, H_2O 1.7 kPa, total pressure 101 kPa, Ar balance, 40 mL min^{-1}. The first reactor; 800 mg of 5 wt% Na_2WO_4/SiO_2 at 850 °C. The second reactor; without catalysts at 850–1000 °C. O_2 is depleted under all the conditions.

$$C_2H_4 \rightarrow C_2H_2 + H_2 \quad \Delta H^0_{298K} = 175 \text{ kJ mol}^{-1} \tag{9}$$

In general, gas phase reactions first require the initiation of radical formation from gas molecules. These radicals successively react with the gas phase molecules and reach a steady-state condition *via* radical propagation reactions. The radical initiation reactions in the present OCM product gas mixture would be the following equations.[36]

$$C_2H_6 \rightarrow 2CH_3^{\cdot} \tag{10}$$

$$2C_2H_4 \rightarrow C_2H_3^{\cdot} + C_2H_5^{\cdot} \tag{11}$$

CH_4 conversion did not change significantly. Since CH_4 is a stable hydrocarbon, pyrolysis reactions under non-oxidative conditions have been reported to proceed only at temperatures above 1200 °C.[37,38] The selectivity to C_{3-5} also did not change significantly, while that to benzene and toluene increased with an increase in temperature in the second reactor, which was due to condensation of C_2H_2.

$$3C_2H_2 \rightarrow C_6H_6 \quad \Delta H^0_{298K} = -600 \text{ kJ mol}^{-1} \tag{12}$$

Graphitic carbon, which is produced after further condensation, was also observed on the quartz tube wall after the reaction. Formation of graphitic carbon is not considered in the calculation of the selectivity due to its negligible amount (<0.1% C selectivity). Since the dehydrogenation and condensation reactions are endothermic and exothermic reactions, respectively, these reactions are expected to be balanced. In the present study, the gas mixture diluted by Ar was investigated. The homogeneous reactions are expected to play an important role in determining the selectivity for the operation at industrially relevant high pressure (>1.0 MPa) in which intense reaction heat is also generated.

In the present experimental study, gas phase reactions are limited to the volume in the quartz tube microreactor (I.D. 4 mm and length approximately 8 cm) whose residence time is approximately 0.6 s. Although our microreactor system has the limitation of varying residence times, in large-scale industrial reactors, the product gas mixture would be exposed to high temperature, potentially for an extended time.[39] Homogeneous gas phase reactions were further simulated under isothermal conditions with an extended residence time in a single plug-flow reactor (PFR) according to the reported gas-phase chemical kinetic model by feeding the OCM products, with experimentally obtained outlet composition from the first reactor. This simulation clarifies the reaction

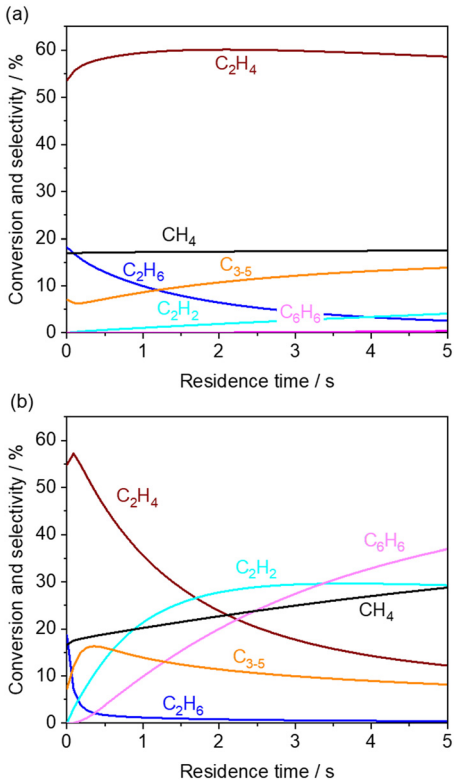

Fig. 4 Simulated product distribution and CH_4 conversion at (a) 850 and (b) 1000 °C using KAM1-GS gas phase kinetics. Inlet gas composition was given by the experimentally obtained values from the outlet of the first reactor. The corresponding mole fractions are shown in Fig. S3.†

pathways in the gas phase without the contribution from the reactor wall, which leads to the change in product distributions.

First, the simulated CH_4 conversion did not change at 850 °C, while it gradually increased at 1000 °C due to pyrolysis (Fig. 4a and b).[23,40] Meanwhile, in our measurement at the residence time of approximately 0.6 s, the CH_4 conversion did not change significantly (Fig. 3). From the rate of production (ROP) analysis in the simulation, the H radical was found to be a major source in the reaction with CH_4. In our experiments using a microreactor, quenching of H radical on the wall of the quartz tube may have occurred, which limited the conversion of CH_4. Alternatively, CH_4 was also formed from the CH_3 radical after abstracting hydrogen from hydrocarbons. These processes of formation and consumption of CH_4 were balanced; thus CH_4 conversion was minimally affected.

The simulated C_2H_6 selectivity decreases rapidly, while the C_2H_2 and C_6H_6 selectivity increases at higher temperatures, which agrees with our experimental observations. ROP analysis at the residence time of 0 s revealed that C_2H_6 is the major source in the radical initiation reactions to produce a radical compared to other hydrocarbons and H_2O in the gas phase. A CH_3 radical was produced from C_2H_6 through eqn (10) with the help of a third body, which leads to the following radical propagation reactions. The third body including inert gas itself is not consumed during the gas phase reactions but influences the reaction rate *via* collision either by providing the energy to form excited intermediates or by dissipating the energy from the excited intermediates after radical recombinations.[41,42] The sharp decay of C_2H_6 selectivity is due to its weak C–H bond strength (423 kJ mol^{-1}) compared to other hydrocarbons (CH_4: 439 kJ mol^{-1}; C_2H_4: 463 kJ mol^{-1}).[43] As the residence time increases, the C_2 products transform to C_2H_2 and C_6H_6 in the simulation. In the present microreactor experimentally used, its volume is limited. However, these transformations may turn out to be significant in industrial reactors with a huge volume and generated heat. Mole fractions of CO and CO_2 did not change significantly (Fig. S3†) by the gas phase kinetics at the simulated temperature and in the residence time range, which is in contrast to the experimental observation shown in Fig. 3. The deviation may be caused by heterogeneous steam reforming concurrently followed by the water gas shift reaction on the wall of the quartz tube, SiO_2, which is discussed in the next section.

The major pathways obtained from ROP analysis in the simulation at 1000 °C and a residence time of 1 s are shown in Fig. 5. Fig. 5a shows the consumption and production cycle of CH_4 during which CH_4 is consumed by an H radical, and CH_4 is regenerated through hydrogen abstraction from the major hydrocarbons *via* the CH_3 radical. This cycle was most likely balanced in our experimental setup resulting in the maintenance of CH_4 conversion. The H radical is formed from the decomposition of unstable hydrocarbon radicals (Fig. 5b). H radical can readily react with CH_4, which is the primary component in the gas phase. Combination of pathways in Fig. 5a and b results in the dehydrogenation of C_2 products to form H_2. H_2 hardly reacts in the gas phase. Hydrogen abstraction by H and CH_3 radicals is the dominant reaction involved in consuming C_2H_6 and the formation of

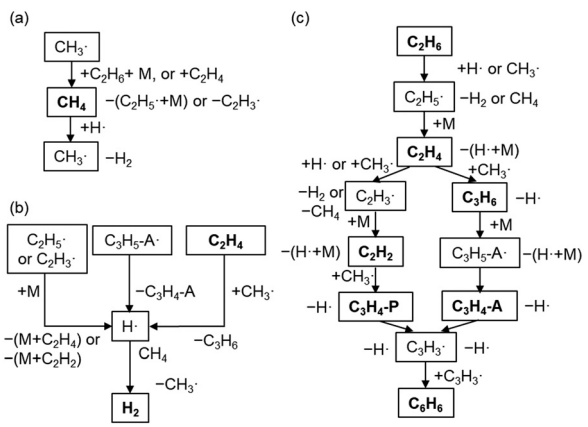

Fig. 5 Major pathways based on the ROP analysis at 1000 °C and a residence time of 1 s. (a) The production and consumption of CH_4, (b) the formation of H radicals and H_2, and (c) the transformation from C_2 products to benzene. M, P, and A represent the third body, propene, and allene, respectively.

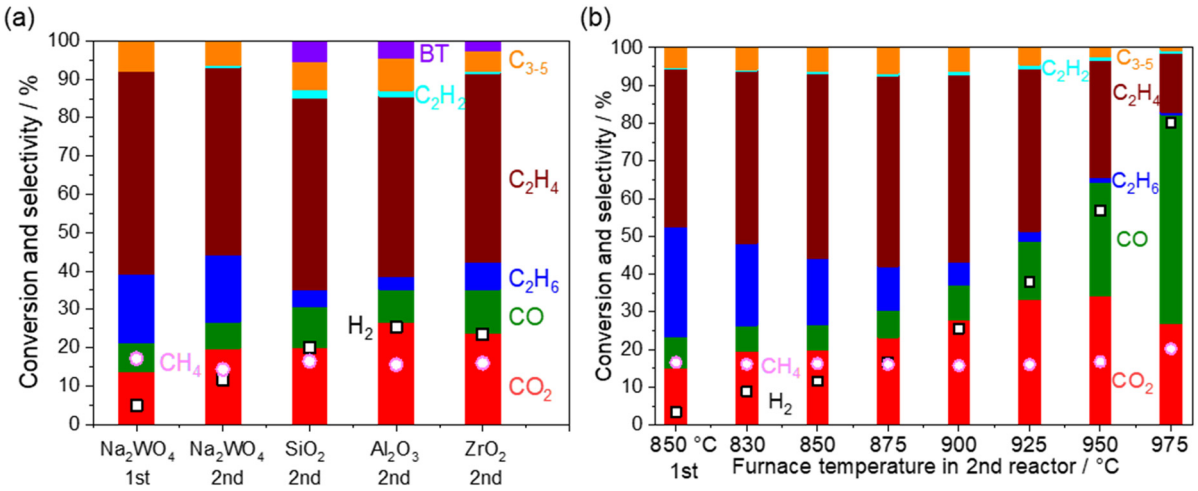

Fig. 6 Product distribution and CH_4 conversion from the outlets of the first and the second reactor. Inlet gas; CH_4 10 kPa, O_2 1.4 kPa, H_2O 1.7 kPa, total pressure 101 kPa, Ar balance, 40 mL min^{-1}. O_2 is depleted under all the conditions. The first reactor: 800 mg of 5 wt% Na_2WO_4/SiO_2 at 850 °C. (a) The second reactor: 800 mg of the catalysts (5 wt% Na_2WO_4/SiO_2) or 500 mg of the supports (SiO_2, Al_2O_3, and ZrO_2) at 850 °C. (b) The second reactor: 800 mg of the catalysts (5 wt% Na_2WO_4/SiO_2) at 830–975 °C.

C_2H_5 radicals, which are further converted into C_2H_4 (Fig. 5c). The majority of C_2H_4 was found to have reacted with the CH_3 radical to form C_2H_3 radicals and C_3H_6. Both of them are converted to C_3H_3 through a couple of radical reactions, which then finally form benzene. C_2H_2 and C_3 products are the intermediate products in this pathway.

Heterogeneous reactions on various catalysts

Heterogeneous reactions on the catalysts and supports after O_2 depletion were further investigated at 850 °C by loading various catalysts and supports (5 wt% Na_2WO_4/SiO_2, SiO_2, ZrO_2, and Al_2O_3) in the second reactor (Fig. 6a). The cristobalite phase, SiO_2, was selected because the SiO_2 support is known to transform into cristobalite at the operating temperature in the presence of Na_2WO_4.[21,28] First, CH_4 conversion remained constant after going through the second reactor, indicating that CH_4 hardly reacts under non-oxidative conditions even in the presence of these materials. After going through the second reactor, the selectivity to CO_x and H_2 was increased at the expense of the C_2 selectivity. Considering that the OCM product mixture also contained water vapor, steam reforming of C_2 products and water gas shift reaction seemed to have occurred.

$$C_2H_6 + 2H_2O \rightarrow 2CO + 5H_2 \quad \Delta H^0_{298K} = 347 \text{ kJ mol}^{-1} \quad (13)$$

$$C_2H_4 + 2H_2O \rightarrow 2CO + 4H_2 \quad \Delta H^0_{298K} = 210 \text{ kJ mol}^{-1} \quad (14)$$

$$CO + H_2O \rightarrow CO_2 + H_2 \quad \Delta H^0_{298K} = -41 \text{ kJ mol}^{-1} \quad (15)$$

Because the increase in the CO_x selectivity was not observed at 850 °C when the second reactor did not contain any catalyst and support (Fig. 3), these reactions seem to have occurred heterogeneously. Surprisingly, the above mentioned reactions occurred even on SiO_2 (cristobalite), ZrO_2, and Al_2O_3, which are often assumed to be inert and commonly used for reactor materials and supports. CO_x formation was slightly suppressed when 5 wt% of Na_2WO_4 was loaded onto the SiO_2. This may be because molten Na_2WO_4 (melting temperature 697 °C) partially covered the surface of SiO_2.[20,25,44,45]

Regarding the reported steam reforming and water gas shift reactions on oxides, Fe_2O_3/Cr_2O_3 and CuO/ZnO are used industrially for water gas shift reactions below 500 °C.[46,47] Their common research direction is to lower the reaction temperature, a process that is thermodynamically preferred for obtaining a high H_2 yield. Steam reforming of ethylene using oxide materials without supported metals has been rarely reported. $NiAl_2O_4$ and $MnCr_2O_4$ spinel oxides, which are candidate barrier layers in hydrocarbon steam crackers to prevent coke formation, were evaluated for the steam reforming of ethylene below 700 °C.[48,49] The present study revealed a unique challenge on oxides after OCM, which operates at high temperature (>800 °C).

The temperature in the second reactor with 5 wt% Na_2WO_4/SiO_2 as the model catalyst was further varied to mimic the extra amount of catalyst exposed at high temperature generated by the exothermic OCM reaction (Fig. 6b). Again, CH_4 conversion remained constant even at 975 °C, indicating the difficulty in activating the stable CH_4 in a non-oxidative environment. CO_x and H_2 selectivities increased significantly after increasing the temperature, whereas C_2 selectivity decreased. Notably, the loss of C_2 selectivity was also observed even at 830 °C, which is below the operating temperature for OCM. A closer look at the results reveals that the consumption of C_2H_6 was greater than the production of CO_x in the temperature range below 950 °C. The selectivity to C_2H_4 increased from the outlet of the first reactor in this temperature range. These observations suggest that the

dehydrogenation of C_2H_6 to C_2H_4 (eqn 5) dominates the consumption of C_2H_6 compared to the steam reforming of C_2H_6 to CO (eqn 13). Therefore, the CO_x formation should originate from the steam reforming of C_2H_4 (eqn 14). Similar interpretations have been previously reported during the steam reforming of C_2H_4 and C_2H_6 using a $Mn_{0.5}Cr_{2.5}O_4$ spinel catalyst operated below 700 °C.[49] The measured H_2 formation in the second reactor agrees with the one estimated from the consumption of C_2H_6 and CO_x formation (see Fig. S4 and ESI† note 1). The steam reforming and the water gas shift reactions seem to be the major H_2 source, particularly at high temperatures.

The water gas shift reaction on the commonly used metal catalysts, such as Ni, Ru, Rh, Pt, and Ir, is known to be reversible and readily reaches equilibrium.[47,50,51] The outlet gas composition from the second reactor was compared with the equilibrium constant of the water gas shift reaction, K_{WGS}, at various temperatures using the equation shown below (Fig. S5†):

$$\eta_{WGS} = \frac{P_{CO_2}P_{H_2}}{P_{CO}P_{H_2O}K_{WGS}} \quad (16)$$

η_{WGS} showed a gradual increase by increasing the furnace temperature due to the enhanced kinetics till its equilibrated value of unity above 900 °C was reached. This result further clarifies that the excess heat needs to be effectively removed after O_2 depletion to avoid the formation of undesired CO_2.

The product gas mixture from the first reactor was directly introduced in the second reactor in this study. Investigations on the heterogeneous reactions for the individual hydrocarbons in the presence of steam would help to further clarify their reaction rates, which can be input parameters when designing industrial reactors.

Overall, the present study revealed significant contributions from the gas phase, catalysts, and reactor materials towards the successive reactions of OCM products under high temperature non-oxidative conditions. Particularly, the catalytic steam reforming and water gas shift reactions, which would occur on an excess amount of catalysts and reactor materials especially at increased temperatures from exothermic reaction, need to be suppressed to prevent undesired CO_x formation. Because OCM is an exothermic reaction, measures to effectively dissipate the excess heat would be needed to prevent any undesired reactions. For example, microchannel reactors with coated catalyst walls are expected to have a high heat transfer coefficient, which is inversely dependent on the tube diameter.[52,53] A co- or counter flow of a coolant can be also introduced within the channels.[54] Alternatively, a monolith structure may facilitate the heat and mass transfer compared to the packed bed reactor.[55] Metallic foams are considered thermally conductive monolith supports.[56–58] Membrane reactors, which provide O_2 gradually along the reaction zone, may prevent the formation of strong hot spots.[59–61] Cooling by endothermic reactions is also proposed, for example, successive steam reforming of unconverted CH_4 to syngas using the reaction heat from OCM,[62] although these reactions may not fully compensate the strong exothermicity from OCM. Additionally, since the steam reforming reaction was also observed below the operation temperature of OCM (Fig. 6b), the residence time in the catalyst bed needs to be carefully controlled. Efforts to improve the stability of the catalyst are highly needed to reduce the excess amount of the catalyst. Since the steam reforming reaction was also observed using ZrO_2 and Al_2O_3, which are commonly used supports as well as reactor materials, the choice of those materials should be avoided or its surface decoration to make it inert is necessary. Operando temperature measurements within the catalyst bed also helps to develop efficient OCM reactors.[63–66]

Conclusions

The present study investigated the successive reactions of OCM products under non-oxidative conditions at high temperatures, which would be generated *via* exothermic heat after depletion of O_2 in industrial reactors. The developed two-stage reactor successfully revealed the contributions from the gas-phase and heterogeneous reactions. In the absence of catalysts and supports, C_2 products dehydrogenate to C_2H_2 followed by condensation to benzene, toluene, and graphitic carbon deposits, which would cause the pressure drop and suppression of heat transfer in OCM reactors. Notably, the steam reforming of the C_2 products and water gas shift reactions were observed to lead to the loss of C_2 yield in the presence of the model catalysts and support materials, which are commonly considered to be inactive. Research efforts should be directed to design an efficient OCM reactor to remove the excess heat generated to prevent the undesired reactions. The residence time also needs be carefully controlled to minimize the extra contact of the C_2 products with catalysts and reactor materials at increased temperature.

Author contributions

Conceptualization, K. T.; investigation H. K., K. O., and D. L.; writing – original draft, H. K. and K. O.; writing – review & editing, K. O., S. M. S. and K. T.; supervision, K. T.; funding acquisition, K. T.

Conflicts of interest

There are no conflicts to declare.

Acknowledgements

This work was supported by MHI Innovation Accelerator LLC.

References

1 M. J. da Silva, *Fuel Process. Technol.*, 2016, **145**, 42–61.
2 P. Schwach, X. Pan and X. Bao, *Chem. Rev.*, 2017, **117**, 8497–8520.

3 J. H. Lunsford, *Angew. Chem., Int. Ed. Engl.*, 1995, **34**, 970–980.
4 J. T. Grant, J. M. Venegas, W. P. McDermott and I. Hermans, *Chem. Rev.*, 2018, **118**, 2769–2815.
5 G. Keller and M. M. Bhasin, *J. Catal.*, 1982, **73**, 9–19.
6 M. Y. Sinev, Z. T. Fattakhova, V. I. Lomonosov and Y. A. Gordienko, *J. Nat. Gas Chem.*, 2009, **18**, 273–287.
7 M. Y. Sinev, *J. Catal.*, 2003, **216**, 468–476.
8 S. Pak, P. Qiu and J. H. Lunsford, *J. Catal.*, 1998, **179**, 222–230.
9 J. A. Labinger and K. C. Ott, *J. Phys. Chem.*, 1987, **91**, 2682–2684.
10 J. A. Labinger, *Catal. Lett.*, 1988, **1**, 371–375.
11 J. S. Lee and S. T. Oyama, *Catal. Rev.: Sci. Eng.*, 1988, **30**, 249–280.
12 C. Batiot and B. K. Hodnett, *Appl. Catal., A*, 1996, **137**, 179–191.
13 J. Song, Y. Sun, R. Ba, S. Huang, Y. Zhao, J. Zhang, Y. Sun and Y. Zhu, *Nanoscale*, 2015, **7**, 2260–2264.
14 D. Noon, A. Seubsai and S. Senkan, *ChemCatChem*, 2013, **5**, 146–149.
15 H. Wang, C. Yang, C. Shao, S. Alturkistani, G. Magnotti, J. Gascon, K. Takanabe and S. M. Sarathy, *ChemCatChem*, 2022, **14**, e202200927.
16 K. Takanabe and E. Iglesia, *Angew. Chem., Int. Ed.*, 2008, **47**, 7689–7693.
17 K. Takanabe and E. Iglesia, *J. Phys. Chem. C*, 2009, **113**, 10131–10145.
18 D. Li, W. S. Baslyman, S. M. Sarathy and K. Takanabe, *Energy Technol.*, 2020, **8**, 1900563.
19 D. Li, S. Yoshida, B. Siritanaratkul, A. T. Garcia-Esparza, D. Sokaras, H. Ogasawara and K. Takanabe, *ACS Catal.*, 2021, **11**, 14237–14248.
20 K. Takanabe, A. M. Khan, Y. Tang, L. Nguyen, A. Ziani, B. W. Jacobs, A. M. Elbaz, S. M. Sarathy and F. F. Tao, *Angew. Chem., Int. Ed.*, 2017, **56**, 10403–10407.
21 A. Palermo, J. Holgadovazquez, A. Lee, M. Tikhov and R. Lambert, *J. Catal.*, 1998, **177**, 259–266.
22 Y. Liang, Z. Li, M. Nourdine, S. Shahid and K. Takanabe, *ChemCatChem*, 2014, **6**, 1245–1251.
23 D. Li, W. S. Baslyman, B. Siritanaratkul, T. Shinagawa, S. M. Sarathy and K. Takanabe, *Ind. Eng. Chem. Res.*, 2019, **58**, 22884–22892.
24 S. Sourav, Y. Wang, D. Kiani, J. Baltrusaitis, R. R. Fushimi and I. E. Wachs, *Angew. Chem., Int. Ed.*, 2021, **60**, 21502–21511.
25 M. J. Werny, Y. Wang, F. Girgsdies, R. Schlögl and A. Trunschke, *Angew. Chem., Int. Ed.*, 2020, **59**, 14921–14926.
26 Z. C. Jiang, C. J. Yu, X. P. Fang, S. B. Li and H. L. Wang, *J. Phys. Chem.*, 1993, **97**, 12870–12875.
27 S. Ji, T. Xiao, S. Li, L. Chou, B. Zhang, C. Xu, R. Hou, A. P. E. York and M. L. H. Green, *J. Catal.*, 2003, **220**, 47–56.
28 D. Kiani, S. Sourav, W. Taifan, M. Calatayud, F. Tielens, I. E. Wachs and J. Baltrusaitis, *ACS Catal.*, 2020, **10**, 4580–4592.
29 D. J. Wang, M. P. Rosynek and J. H. Lunsford, *J. Catal.*, 1995, **155**, 390–402.
30 D. Kiani, S. Sourav, J. Baltrusaitis and I. E. Wachs, *ACS Catal.*, 2019, **9**, 5912–5928.
31 C. Guéret, M. Daroux and F. Billaud, *Chem. Eng. Sci.*, 1997, **52**, 815–827.
32 F. Larkins and A. Khan, *Aust. J. Chem.*, 1989, **42**, 1655.
33 S. M. Burke, W. Metcalfe, O. Herbinet, F. Battin-Leclerc, F. M. Haas, J. Santner, F. L. Dryer and H. J. Curran, *Combust. Flame*, 2014, **161**, 2765–2784.
34 W. K. Metcalfe, S. M. Burke, S. S. Ahmed and H. J. Curran, *Int. J. Chem. Kinet.*, 2013, **45**, 638–675.
35 D. Darcy, H. Nakamura, C. J. Tobin, M. Mehl, W. K. Metcalfe, W. J. Pitz, C. K. Westbrook and H. J. Curran, *Combust. Flame*, 2014, **161**, 65–74.
36 K. M. Sundaram and G. F. Froment, *Ind. Eng. Chem. Fundam.*, 1978, **17**, 174–182.
37 A. Holmen, O. Olsvik and O. A. Rokstad, *Fuel Process. Technol.*, 1995, **42**, 249–267.
38 U. P. M. Ashik, W. M. A. W. Daud and H. F. Abbas, *Renewable Sustainable Energy Rev.*, 2015, **44**, 221–256.
39 G. Radaelli, G. Chachra and D. Jonnavittula, *Low-Energy, Low-Cost Production of Ethylene by Low- Temperature Oxidative Coupling of Methane*, United States, 2017.
40 H. B. Palmer, J. Lahaye and K. C. Hou, *J. Phys. Chem.*, 1968, **72**, 348–353.
41 M. Y. Sinev, Y. P. Tulenin, O. V. Kalashnikova, V. Y. Bychkov and V. N. Korchak, *Catal. Today*, 1996, **32**, 157–162.
42 M. Sinev, V. Arutyunov and A. Romanets, *Adv. Chem. Eng.*, 2007, **32**, 167–258.
43 S. J. Blanksby and G. B. Ellison, *Acc. Chem. Res.*, 2003, **36**, 255–263.
44 Z. C. Jiang, C. J. Yu, X. P. Fang, S. B. Li and H. L. Wang, *J. Phys. Chem.*, 1993, **97**, 12870–12875.
45 Z. Q. Yu, X. M. Yang, J. H. Lunsford and M. P. Rosynek, *J. Catal.*, 1995, **154**, 163–173.
46 C. Rhodes, G. J. Hutchings and A. M. Ward, *Catal. Today*, 1995, **23**, 43–58.
47 S. Hla, D. Park, G. Duffy, J. Edwards, D. Roberts, A. Ilyushechkin, L. Morpeth and T. Nguyen, *Chem. Eng. J.*, 2009, **146**, 148–154.
48 L. Yang, M. P. Bukhovko, A. Malek, L. Li, C. W. Jones, P. K. Agrawal and R. J. Davis, *Appl. Catal., A*, 2020, **603**, 117739.
49 L. Yang, M. P. Bukhovko, G. Brezicki, A. Malek, L. Li, C. W. Jones, P. K. Agrawal and R. J. Davis, *J. Catal.*, 2019, **380**, 224–235.
50 J. Wei and E. Iglesia, *J. Phys. Chem. B*, 2004, **108**, 4094–4103.
51 A. Yamaguchi and E. Iglesia, *J. Catal.*, 2010, **274**, 52–63.
52 R. Knitter and M. A. Liauw, *Lab Chip*, 2004, **4**, 378.
53 T. Serres, L. Dreibine and Y. Schuurman, *Chem. Eng. J.*, 2012, **213**, 31–40.
54 I. Tezcan and A. K. Avci, *J. Chem. Technol. Biotechnol.*, 2015, **90**, 1827–1838.
55 G. Groppi and E. Tronconi, *Chem. Eng. Sci.*, 2000, **55**, 2161–2171.
56 M. Bracconi, M. Ambrosetti, M. Maestri, G. Groppi and E. Tronconi, *Chem. Eng. Process.*, 2018, **129**, 181–189.

57 L. Giani, G. Groppi and E. Tronconi, *Ind. Eng. Chem. Res.*, 2005, **44**, 9078–9085.
58 C. G. Visconti, A. Montebelli, G. Groppi, E. Tronconi and S. Kohler, in *Methanol*, Elsevier, 2018, pp. 519–538.
59 H. R. Godini, S. Xiao, M. Kim, N. Holst, S. Jašo, O. Görke, J. Steinbach and G. Wozny, *J. Ind. Eng. Chem.*, 2014, **20**, 1993–2002.
60 M.-S. Salehi, M. Askarishahi, H. R. Godini, O. Görke and G. Wozny, *Ind. Eng. Chem. Res.*, 2016, **55**, 3287–3299.
61 N. Holst, S. Jašo, H. R. Godini, S. Glöser, H. Arellano-Garcia, G. Wozny and J. Steinbach, *Chem. Eng. Technol.*, 2012, **35**, 294–301.
62 T. P. Tiemersma, T. Kolkman, J. A. M. Kuipers and M. van Sint Annaland, *Chem. Eng. J.*, 2012, **203**, 223–230.
63 S. Pak and J. H. Lunsford, *Appl. Catal., A*, 1998, **168**, 131–137.
64 B. Zohour, D. Noon and S. Senkan, *ChemCatChem*, 2013, **5**, 2809–2812.
65 D. Noon, B. Zohour and S. Senkan, *J. Nat. Gas Sci. Eng.*, 2014, **18**, 406–411.
66 O. Korup, S. Mavlyankariev, M. Geske, C. F. Goldsmith and R. Horn, *Chem. Eng. Process.: Process Intesif.*, 2011, **50**, 998–1009.